LAWRENCE
LIVERMORE
NATIONAL
LABORATORY

LLNL-JRNL-609316

Effect of Thermal Anneal on Growth Behavior of Laser-Induced Damage Sites on the Exit Surface of Fused Silica

R. N. Raman, R. A. Negres, M. J. Matthews, C. W. Carr

January 3, 2013

Optical Materials Express

Disclaimer

This document was prepared as an account of work sponsored by an agency of the United States government. Neither the United States government nor Lawrence Livermore National Security, LLC, nor any of their employees makes any warranty, expressed or implied, or assumes any legal liability or responsibility for the accuracy, completeness, or usefulness of any information, apparatus, product, or process disclosed, or represents that its use would not infringe privately owned rights. Reference herein to any specific commercial product, process, or service by trade name, trademark, manufacturer, or otherwise does not necessarily constitute or imply its endorsement, recommendation, or favoring by the United States government or Lawrence Livermore National Security, LLC. The views and opinions of authors expressed herein do not necessarily state or reflect those of the United States government or Lawrence Livermore National Security, LLC, and shall not be used for advertising or product endorsement purposes.

Effect of thermal anneal on growth behavior of laser-induced damage sites on the exit surface of fused silica

Rajesh N. Raman, Raluca A. Negres, Manyalibo J. Matthews, and Christopher W. Carr
Lawrence Livermore National Laboratory, 7000 East Ave, Livermore, CA, USA 94550

ABSTRACT

Thermal anneal is known to arrest the growth of laser-induced damage in optical materials. However, the response of the material which leads to this observed behavior is poorly understood. In this work, we investigate the effect of isothermal anneal at 1100°C for 12 hours on the growth rate of laser-induced damage sites in fused silica. Growth rate was significantly lower for annealed initiated damage sites than that for untreated sites. This decrease in growth rate was associated with the closure of small surface and subsurface cracks, suggesting that aggressive growth rate is due, at least in part, to subsurface fracture complexity.

Subject Terms: Thermal anneal, laser damage, damage growth, fused silica

I. INTRODUCTION

While advances have been made in bulk purification and surface finishing methods for optical materials [(Menapace, Penetrante et al. 2002), (Suratwala, Miller et al. 2011)], localized damage on optical components used in high power laser systems continues to limit their operational lifetime. The initial size of such damage sites is highly dependent on laser conditions [(Carr, Trenholme et al. 2007), (Carr, Cross et al. 2011)] but range from a few microns to a few tens of microns for nanosecond pulses. As initiated, these sites are sufficiently sparse that they would pose no significant threat to beam throughput were it not for their propensity to grow exponentially in diameter upon exposure to subsequent pulses (*damage growth*) [(Norton, Hrubesh et al. 2001), (Raze, Morchain et al. 2003), (Huang, Han et al. 2009), (Negres, Norton et al. 2010)]. Thus, the study of the nature of damage growth is of great interest in terms of 1) understanding the fundamental response of optical materials to laser energy deposition and 2) impeding and possibly arresting such growth behavior. In working towards these goals, it has been observed that a number of parameters affect the rate at which sites grow (laser fluence, pulse duration, and wavelength, as well as site morphology). Moreover, sites with nominally identical diameter exposed to nearly identical laser pulses can grow at different rates, and the distributions of these growth rates have been documented [(Negres, Norton et al. 2009)]. This observation requires that additional innate characteristics of the site, apart from surface diameter, govern growth behavior. To date it is unknown which damage site attributes lead to more aggressive growth; however, it has been observed that individual damage sites can substantially differ structurally, such as in crater morphology and surrounding crack network [(Wong, Ferriera et al. 2006), (Hu, Zhao et al. 2010), (Carr, Matthews et al. 2007), (Negres, Norton et al. 2010)]. Furthermore, previous work has suggested an association between structural properties and propagation of flaws in glass [(Hrma, Han et al. 1988), (Dahmani, Lambropoulos et al. 1999), (Matthews, Stolken et al. 2009)]. Thus, damage site structure may relate to how fast it will grow upon subsequent laser exposure.

Traditionally, structural properties of ceramic materials, (e.g., ZnO, Al_2O_3, and MgO) have been probed by thermal anneal [(Lange and Gupta 1970), (Gupta 1984)]. More recently, thermal anneal has been shown to improve optical transmission and laser-induced damage threshold of ceramics as diverse as ZnSe crystals [(Zagoruiko 1999)], potassium dihydrogen phosphate [(Swain, Stokowski et al. 1982), (Atherton 1994)], oxide thin films [(Milam, Lowdermilk et al. 1982), (Tian, Huang et al. 2005)], and fused silica [(Shen 2012), (Laurence, Bude et al. 2009)]. A study on the isothermal anneal of indenter-generated cracks in silica showed partial crack healing at temperatures as low as 525°C in the form of crack pinching and crack tip blunting

driven by capillary flow [(Hrma, Han et al. 1988)]. Increasing the anneal temperature and time revealed a treatment regime of strengthening followed by weakening.

Thermal anneal of laser-induced damage on SiO_2 surface has also been achieved by exposure to 10.6 μm wavelength CO_2 laser irradiation (SiO_2 absorption coefficient ~10^3 cm^{-1}), leading to significant surface smoothing and an arrest of growth [(Temple, Lowdermilk et al. 1982), (Brusasco, Penetrante et al. 2002)]. While CO_2 laser heating permits the observation of local, *in situ* healing of damage sites [(Yang, Matthews et al. 2010)], in this study we employ an oven anneal for simultaneous treatment of a large number of sites at identical conditions which is necessary for elucidating the statistical nature of damage growth. In addition to treatment homogeneity, an oven treatment generates smaller spatial thermal gradients and subsequently less residual stress than that compared to a spatially finite CO_2 laser beam. The primary metric we employ to characterize growth behavior is the rate at which a damage site grows laterally following a laser shot (*growth rate*). In this work, we investigate the effect of isothermal anneal on growth rate of both as-initiated and grown damage sites. Furthermore, we explore the relationship between growth rate and measurable anneal-induced changes in surface and sub-surface damage structure, relative concentration of ultraviolet (UV) light absorbers, and stress-induced birefringence, in reference to the known thermal properties of fused silica.

II. EXPERIMENTAL PROCEDURE

2.1 Sample preparation

Two UV-grade fused silica rounds (Corning 7980, [OH] ~1000 ppm wt. %) were used in this study. Sample A, intended for large aperture damage growth, was 1 cm in thickness and 2 inches in diameter. Sample B, intended for side-viewing of damage site features extending from the surface into the bulk, began as an identical cylinder and was then cut to produce a 1-cm thick square with rounded corners. By keeping the corners rounded the sample could still be held in standard 2-inch optics mounts. All four edges were polished to allow imaging though the sides of the sample.

Both samples were then exposed to a chemical etchant to render the surfaces with state-of-the-art resistance to laser-induced damage [(Suratwala, Miller et al. 2011)]. Damage sites were initiated on the bare surface using a 1-mJ, single laser pulse from a 355 nm, 3.5-ns Full Width at Half Maximum of intensity (FWHM) Gaussian pulsed laser operating at 10 Hz (EKSPLA). The laser beam was focused down to a ~50 μm diameter spot at the exit surface of the flat using a 300 mm focal lens. The laser fluence at the sample's surface exceeded the surface damage threshold (~60 J/cm^2) and resulted in damage with ~100% probability. The damage manifested itself mostly as single pits with a diameter of 40 ± 10 μm (mean ± standard deviation). Each sample was translated to expose a pristine location to each subsequent pulse. For Sample A, a grid of damage sites was generated across the surface within a 20 mm x 20 mm region of interest located centered on the round [(Laurence, Bude et al. 2012)]. To establish an internal control, initially only one set (5 rows) of damage sites (n=50 with 2 mm nearest neighbor spacing) was created on the lower half of this region of interest (designated as Set 1 or control). In this manner, site growth characteristics before heat-treatment could be determined. For Sample B, one row of damage sites per edge was initiated 5 mm from the edge, yielding a total of 40 sites with 2 mm nearest neighbor spacing.

Following initiation using the small laser beam, the damage sites on Sample A were simultaneously grown using a large aperture (~30 mm) laser beam at the Optical Sciences Laboratory at LLNL. This laser, described in detail elsewhere [(Nostrand, Weiland et al. 2003)] is a Nd:glass amplifier laser system outputting a 3rd harmonic, 100 J pulse tunable in width and shape. Damage growth proceeded in near-vacuum (<10^{-6} Torr) and at room temperature by exposing the sample to a series of five, nearly identical laser pulses at 351-nm, 10.0 ± 2.0 J/cm^2 (mean ± SD), 5-ns flat-in-time (FIT). For each growth shot, the spatial distribution of the fluence within the large aperture beam was recorded and subsequently registered to the sample, providing the local fluence at each site (standard error ~1% of the mean value obtained by averaging over a 500 μm x 500 μm square patch). Between laser exposures, the sites were characterized with a number of methods described in §2.2. Upon completion of the damage growth sequence and site characterization, additional sites (n=60) were initiated as described above in the remaining half of the region of interest (designated as Set 2).

Following thermal anneal, this sample (including sites from both Set 1 and Set 2) were then simultaneously exposed to five additional laser shots at the same fluence to determine growth rate, as described above.

The thermal anneal consisted of heating the samples in an oven at a rate of 10°C/minute from room temperature to 1100°C, then an isothermal hold for 12 hours with steady-state fluctuation of ± 1°C, followed by a 0.5°C/minute cool down back to room temperature. This peak temperature was chosen to slightly exceed the annealing point (1042°C) [(Corning 2003)] at which its shear relaxation time $\tau = \eta(T)/G \sim 2$ minutes, where η is the temperature-dependent viscosity ($\sim 10^{12}$ Pa·s) and G is the shear modulus (30 GPa) [(Zandian, Florry et al. 1991), (Scherer 1992)].

2.2 Diagnostic imaging

After each laser exposure of the damage growth protocol, optical micrographs of each site were acquired using a robotic microscope under back-illumination (LED emission centered at 532 nm) and oblique-illumination (white light). The field of view is 680 x 510 μm, ~2 μm resolution) (Benchmark 200, View Microscopy and Metrology) using a 20X objective with 0.42 NA, 20 mm working distance, and 1.6 μm depth of field (ELWD 20X, Motic). From these images, the effective circular diameter (ECD) and other morphological features of the sites were characterized. The ECD is defined as the diameter of a circle with area equal to that of the damage site and is inferred by thresholding the image beyond the background intensity level.

Each damage site on Sample B, the side cut-and-polished sample, was imaged through at least one polished side. Similar light settings as those for top view measurements were employed for side-view imaging. Images were captured by the robotic microscope both before and after anneal in order to determine the sub-surface morphological response of initiated (small) damage sites.

In addition to optical microscopy, images of sites before and after the anneal were obtained using a scanning electron microscope (SEM) (S3400-N, Hitachi) in order to record sub-micron features on the damage site surface that may be altered by the treatment. The SEM was set at 2.5kV and emission current of 70 μA. Sites were imaged (resolution = 0.07 μm for small sites, 0.10 μm for large sites, averaged over 32 scans (total exposure time per site ~1 minute) in vacuum ($<10^{-5}$ Torr). These settings were not found to have any perceivable effect on the growth rate of damage sites in a separate control experiment.

The robotic microscope was temporarily outfitted with a linear polarizer downstream of the backlight source for polarimetry. The light transmitted through the sample was filtered with a second linear polarizer oriented perpendicular to the input polarization state. This geometry allows imaging of stress-induced birefringence in a dark-field configuration for increased sensitivity, (*i.e.*, no signal when the surface and bulk of a sample are pristine). Depolarized light reaches the detector by either 1) scattering off of multiple surfaces where the ensemble average polarization state is randomized (as can occur when light is scattered by the complex morphology of the damage site) or 2) stress-induced birefringence (as can occur in the volume surrounding the damage site). The difference in the principal stress components normal to the direction of transmitted light propagation can be estimated by

$$\Delta\sigma = (\lambda/(2\pi Cd)) * \cos^{-1}[1 - 2*I_1/I_0] \quad (1)$$

where λ is the source wavelength, C is the stress optic coefficient (35 nm/cm*MPa for fused silica), d is the depth of the volume of material in which birefringence has been induced, I_0 is the source intensity, and I_1 is the maximum intensity in the cross-polarized image arising from birefringence [(Scherer 1992)].

Photoluminescence measurements were performed using a PL microscope apparatus previously described [(Raman, Matthews et al. 2010)]. In brief, sites were exposed to 355 nm laser illumination (1 mW) off-axis for 30 sec while the 420 nm long-pass filtered emission was imaged with resolution on the order of 2 μm onto a liquid nitrogen-cooled CCD camera. This emission is known to originate primarily from the following electronic defects in fused silica: non-bridging oxygen hole centers (NBOHC, peak emission at 650 nm) and laser-induced defects (LID, peak emission at 560 nm) [(Skuja 1998), (Kucheyev and Demos 2003)]. The

mean PL intensity count rate (defined as the ratio of the mean PL counts to UV laser exposure time) from each image was calculated over a circular region of interest with diameter equal to the damage site ECD.

2.3 Determination of growth rate and growth probability

Growth was defined as an event when the site's effective circular diameter ECD_n after shot *n* exceeded its pre-shot diameter ECD_{n-1} by at least 2 μm. This criterion is derived from the resolution of the measurement of site diameter using our imaging system [(Negres, Norton et al. 2010)2010]. In this manner, multiple shots on the same site were treated as independent events in order to generate a population size adequate for reliable statistical analysis of growth rate (this treatment is supported in [(Negres, Norton et al. 2010)]). For example, 66 sites were grown with 5 large aperture shots, resulting in 66 x 5 = 330 exposed sites. Since in that study it was found that growth rate is influenced by ECD and fluence, the exposed sites were binned in these categories: 30-50, 50-70, 70-100, and 100-200 μm bins for ECD and 10 ± 1 J/cm^2 for local fluence. Exposures with fluence outside of the 9-11 J/cm^2 bin were discarded from analysis since sample sizes were insufficient for reliable statistical analysis.

Single-shot growth rate α was calculated based on the expectation of exponential increase in ECD upon exposure to multiple, 5-ns duration laser pulses [(Negres, Norton et al. 2010)]:

$$\alpha = \ln(ECD_n/ECD_{n-1}) \quad (2)$$

A reliable estimation of the likelihood with which a population of exposed sites grows *(probability of growth)* requires analysis of a larger sample size and, for a general description, sampling over a wider fluence range [(Negres, Abdulla et al. 2012)]. Nonetheless, probability of growth was estimated in this study as the fraction of growing exposed sites of comparable diameter (± 10 μm) and laser exposure fluence (± 1 J/cm^2). Binning by size reduces the influence of the previously observed dependence of probability of growth on site diameter, where it was found that smaller sites have a lower probability of growth for a given 351 nm laser fluence [(Negres, Abdulla et al. 2012)].

III. RESULTS

3.1 Growth behavior prior to anneal

The bake itself was found to have no statistically significant effect on the ECD of either the as-initiated or the grown sites ($p = 0.70$ and 0.15, respectively, unpaired t-test). Figure 1(a) shows the progression of the growth rate of the control (unannealed) exposed site population (Sample A, Set 1) as well as that of the annealed exposed site population (Sample A, Set 2) vs. shot number. Since site size varies from shot to shot, the ECD bin is noted for each shot in Fig. 1. Before comparing the growth behavior of annealed vs. control exposed sites, a comment on size bin is warranted. From shot 2 onwards for both populations, a progressive decrease in growth rate (independent of anneal) is observed towards the nominal value (~0.2) measured in previous work (after 30 shots at 10 J/cm^2) [(Negres, Norton et al. 2010)]. Since the mean site ECD gets progressively larger with each laser shot, the cause for this shot-to-shot decrease in growth rate is a function of size. One way to minimize size effects is to grow sites at lower fluences so as to keep them within the same size range and monitor growth behavior over successive shots; however the smaller change in size associated with the lower growth rate would compromise the signal-to-noise ratio of the experiment.

All exposed sites in the unannealed population grew on the first shot, while 2 out of 43 annealed exposed sites (~5%) did not grow. These non-growing sites ($\alpha = 0$) were excluded from analysis of growth rate. For the first shot, annealed exposed sites exhibited a statistically significant reduction in growth rate ($p<0.0001$, unpaired t-test) compared to that of control exposed sites. For the second shot, the difference in mean growth that the effects of the anneal have been fully reversed after this point. Also, control exposed sites 100-200 μm (Set 1) at shot 5 were growing at $\alpha = 0.23 \pm 0.07$ compared to $\alpha = 0.19 \pm 0.02$ immediately after anneal (Fig.

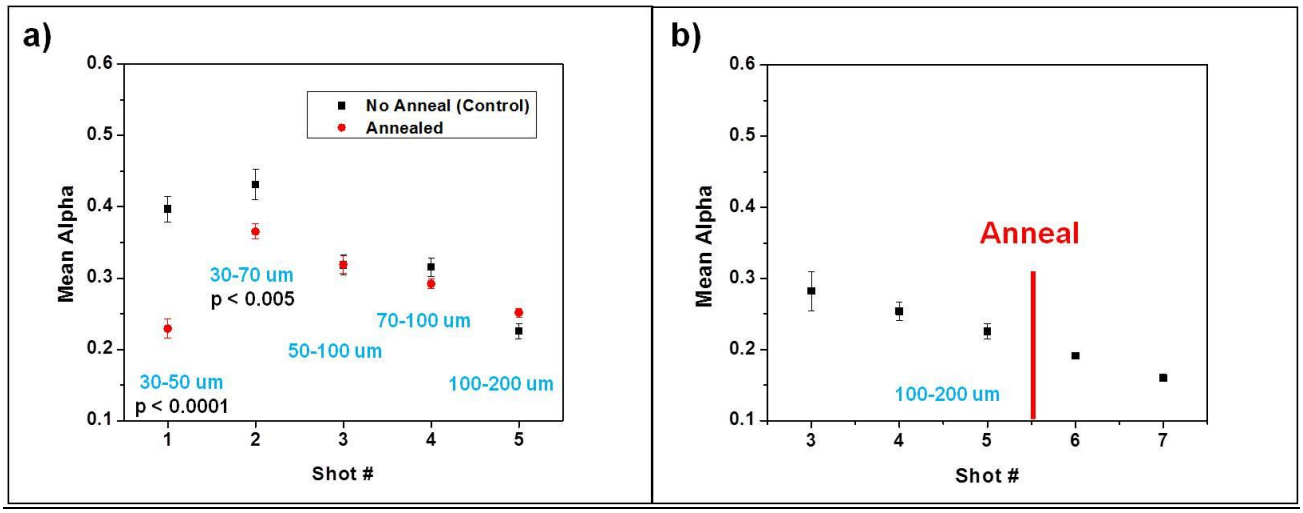

Figure 1. (a) Shot-by-shot progression under 10 ± 1 J/cm^2, 351 nm laser fluence of growth rate (mean ± standard error) of damage sites annealed at 1100°C for 12 hours (circles) compared to that of unannealed sites (squares). (b) Progression of growth rate of large sites (100-200 μm ECD) before and after anneal. Diameter range for sites in each shot is indicated.

1(b)); while a reduction in the mean growth rate of growing sites before and after anneal is apparent, this difference is much less significant ($p<0.02$).

For the remainder of this section, we examine several attributes that may explain this difference in growth response to anneal observed in initiated vs. growing sites. Figure 2 shows typical polarimetry images captured before and after anneal for two damage sites with diameters of 175 um (a-b) and 40 um (c-d). The larger damage site was part of Set 1, grown with 5 laser shots at ~10 J/cm^2, while the smaller site is representative of as-initiated damage sites in Set 2. It was observed that the signal coming from the center of the damage site is somewhat reduced, while the signal at the periphery is almost completely absent after anneal (detection limit of the normalized stress difference $\Delta\sigma/d^{-1}$ ~0.05 MPa/cm^{-1}). This normalized stress difference is used since the actual birefringent (stressed) depth for the damage sites was not determined. These images were contrast-enhanced to highlight the stressed peripheral regions at the expense of saturating the scattered signal from the core. The near-elimination of signal at the periphery upon anneal, where a maximum normalized difference in principal stress was estimated to be ~0.45 ± 0.10 MPa/cm^{-1}, signifies that the employed anneal protocol substantially relaxed the stress in the bulk generated by the growth of the damage site. Reduction of signal coming from the core occurred partially by a smoothing of damage site morphology (and subsequent decrease in scattering, as confirmed by oblique light scattering images, see below) and partially by relaxing stress existing in the volume beneath the damage site. While little stress was detected with this microscope in as-initiated sites (ECD ~40 μm) to begin with (Fig. 2(c)), a reduction in signal from beneath the damage site was observed after anneal (Fig. 2(d)). Thus, both large and small sites alike did not exhibit any significant amount of stress-induced birefringence following anneal. This result is by design, as the oven temperature was chosen to exceed the glass annealing temperature and permit local stress relaxation, while cooling down slowly enough to avoid quenching in a higher fictive temperature and introducing additional stress.

Figures 2(e-h) display typical photoluminescence images of (e-f) a grown site (290 μm ECD) and (g-h) an as-initiated site (40 μm ECD) on a pseudo-color scale before and after anneal. Larger sites exhibit a greater mean PL intensity, likely due to a greater density of electronic defects and/or the larger depth of defective material contributing to the detected signal (if we assume the emission lifetime has not changed significantly). For both large and small sites, concentration of electronic defects (absorbing at 355 nm radiation) was significantly reduced (80% reduction for large sites, 70% reduction for small sites) following anneal, leaving some residual concentration of defects (again, assuming unchanged lifetime). A large reduction in the concentration of point defects was expected at this temperature since point defects are known to annihilate at temperatures as low as a few hundred degrees Celsius [(Primak and Szymanski 1956), (Devine 1990),

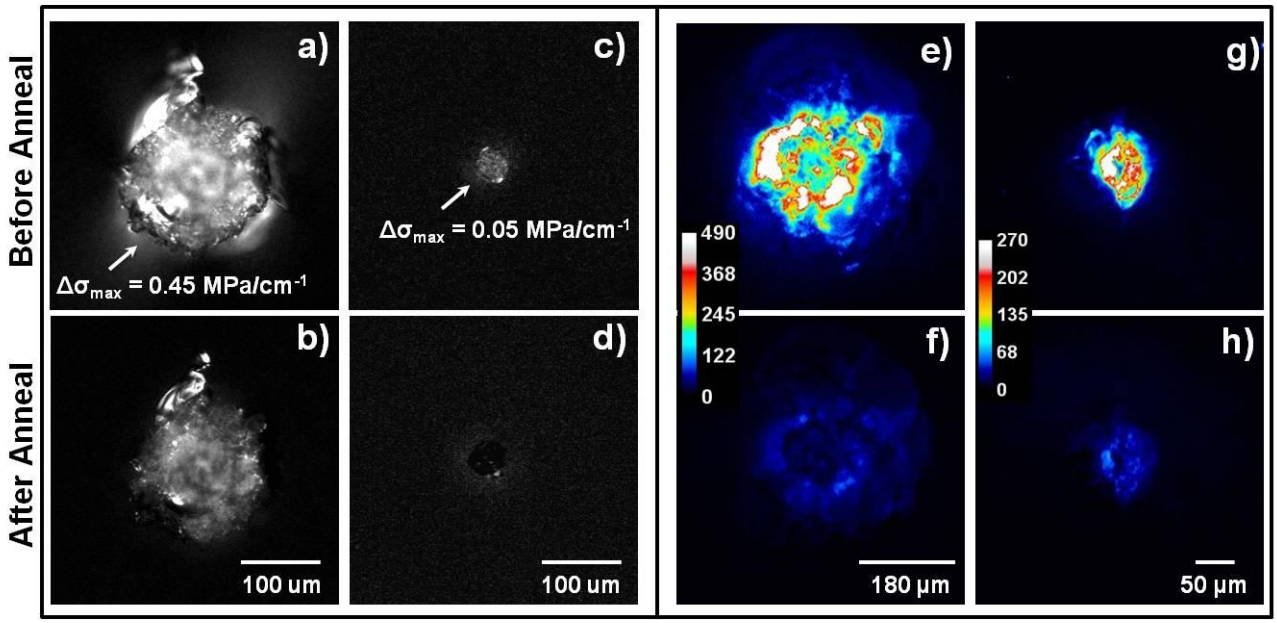

Figure 2. Response to anneal of stress-induced birefringence (a-d) and photoluminescence (pseudo-color) under 355 nm excitation (e-h): (a-b) and (e-f) are images of grown damage sites, (c-d) and (g-h) are images of as-initiated damage sites. Arrows point to regions of maximum birefringence outside of the damage core.

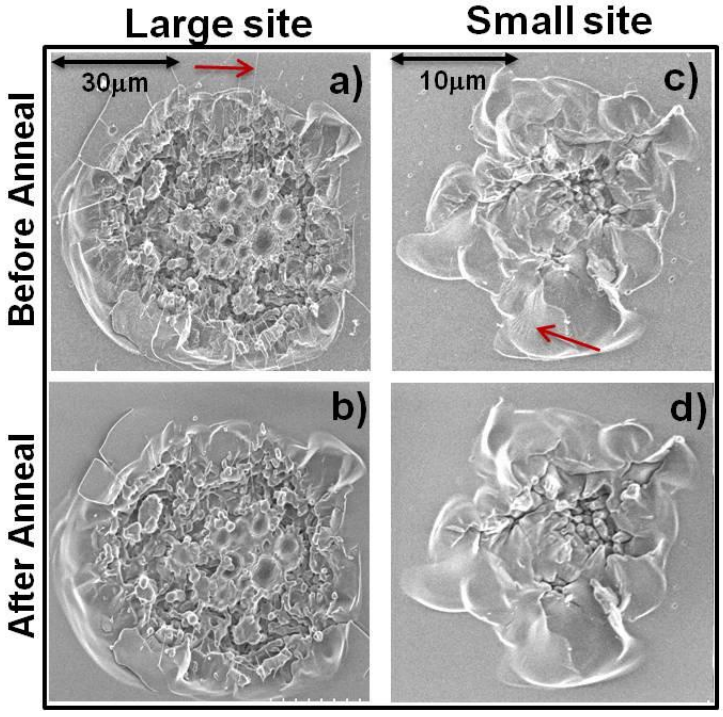

Figure 3. Comparison of SEM images of a site before and after anneal for grown (a-b) and as-initiated (c-d) sites. Top arrow (a) indicates a nanofiber, while bottom arrow (c) indicates hackle.

(Juodkazis, Watanabe et al. 2000), (Shen 2012)].

Figure 3 shows SEM images revealing the response of the surface of both a large and small damage site to anneal. The smoothing of fibers up to 150 nm in width and as thin as 100 nm (see arrow, Fig. 3(a)) is observed. These fibers are believed to have been material liquefied in the high-temperature core during

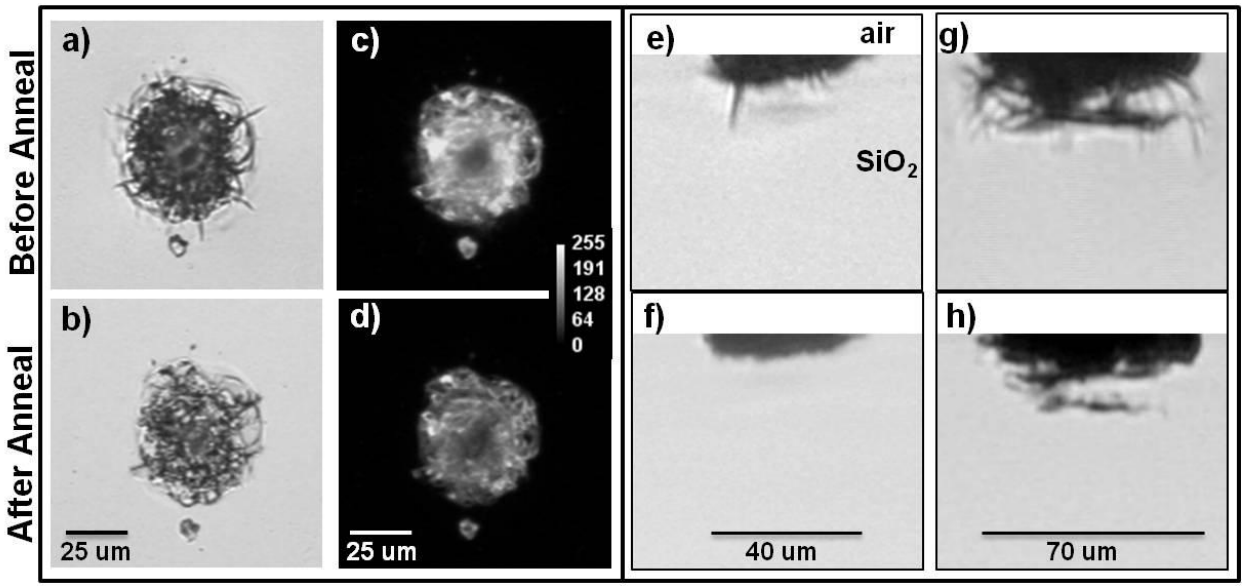

Figure 4. Top-view (a-d) and side-view (e-h) images showing light scattering response to anneal for sites with different ECD. (c-d) oblique light scattering, the rest of the images backlit.

the damage event and pulled behind ejected material [(Carr, Radousky et al. 2004)]. As the fibers cooled, they retained their fibrous shape. In the lower portion of the images of the small site before anneal (see arrow, Fig. 3(c)), 100 nm-wide striations known as hackle can be observed and which smooth upon anneal. From these images it is seen that no smoothing of features on the crater surface larger than ~150 nanometers is observed due to anneal.

Figures 4(a-f) show the response of light scattering from as-initiated damage sites to anneal under backlight and oblique light scattering configurations. Top-view backlit images (Figs. 4(a-b)) reveal the disappearance of surface radial cracks up to 3 μm thick and 15 μm long, thinning of wider cracks, and a recession in the radius of subsurface fracture. In addition, the anneal induced a ~14% decrease in mean oblique light scattering intensity (Figs. 4(c-d)). This reduction could be due to the smoothing of the crater surface rubble as well as to the scattering from subsurface voids and cracks. However, images from SEM have confirmed that no significant smoothing of the crater floor was detected, and the size of features that were smoothed (<150 nm) are too small to efficiently scatter visible light. Thus it is more probable that a reduced amount of crack and fracture is responsible for the reduced oblique light scattering. Figures 4(e-h) show side-view of backlit damag sites revealing the response of the subsurface crack network to anneal. One can identify the closure of subsurface lateral cracks in the bulk up to 9 μm thick and 45 μm long. However, these images also reveal incomplete closure of subsurface fracture as seen in the large sites (Figs. 4(g-h)).

IV. DISCUSSION

This study showed that a thermal anneal of 1100°C produces a pronounced reduction in the growth rate of freshly initiated sites but not in sites which have been grown with several laser exposures. A number of mechanisms have been proposed for damage site growth which may explain this discrepancy: namely residual stress which drives crack propagation, the sub-bandgap absorption of the incident pulse energy by electronic defects [(Skuja 1998)], field intensification brought about by surface roughness [(Genin, Salleo et al. 2001)], and reduced mechanical strength due to the presence of cracks [(Dahmani, Lambropoulos et al. 1999)]. Next, we investigate the differences in how these phenomena present themselves in as-initiated sites versus sites with a number of laser exposures in order to try to explain the difference in growth rate following anneal.

4.1 Residual stress

The choice of 1100°C for the hold temperature of the anneal protocol allowed selective interrogation of these features believed to be responsible for laser-induced growth. As this temperature resides above the glass transition temperature for type III silica glass, any residual stress in the damage sites was allowed to locally relax. For example, the shear relaxation time associated with a 12-hour, 1100°C anneal implies a reduction in stress σ/σ_0 to a value of $\text{Exp}[-t/\tau] = \text{Exp}[-12 \text{ hrs}/0.005 \text{ hrs}] \sim 0$. The substantial reduction in stress-induced birefringence in both as-initiated and grown sites confirms this response, and therefore does not explain the difference in growth behavior observed for as-initiated versus grown sites. Additionally, we consider that the anneal probably depleted some of the OH content at the surface, rendering the volume surrounding the surface-bound region of the damage site stiffer than the volume located further into the bulk. This difference in viscosity could also provide a difference in the amount of stress relaxation around the cracks of initiated vs. grown, deeper sites. Assuming a substantial reduction in [OH] down to ~3 ppm wt. % and estimating the corresponding viscosity [(Zandian, Florry et al. 1991)], the stress would relax to $\sigma/\sigma_0 = \text{Exp}[-12 \text{ hrs}/0.42 \text{ hrs}]$ which is still ~0; due to the chosen anneal hold time, this effect is negligible.

4.2 Photoluminescence

Point defects allow a possible mechanism of energy transfer from the sub-bandgap laser pulse to the silica. Annealing of these defects has been well documented to be driven primarily by diffusion and has been observed to occur efficiently at temperatures well below that employed in this study (~500°C or less) [(Primak and Szymanski 1956), (Devine 1990), (Juodkazis, Watanabe et al. 2000), (Shen 2012)]. In the present work, a 12 hour anneal at 1100°C dramatically reduced the photoluminescence signal, which indicates that the concentration of absorbing defects capable of absorbing UV light is reduced, but not eliminated in both as-initiated and grown sites. This common response in PL emission intensity to anneal for both of these populations suggests that the presence of absorbing defects is not responsible for the observed dissimilarity in growth rate for these 2 populations following anneal.

4.3 Surface smoothing

We turn now to analysis of the morphological changes of damage sites observed in this study. An estimate of the size of features expected to be smoothed due to capillary-driven relaxation can be made (neglecting diffusion and evaporation) using the following relation [(Mullins 1959)]:

$$L = \int \gamma dt/\eta[T(t)] \sim \gamma\pi\tau/\eta \qquad (3)$$

where L is the feature length, γ the surface tension, η the viscosity (a function of temperature and time), and τ the relaxation time (taken here as the anneal hold time). Using published values for γ (0.3 N/m) [(Parikh 1958)] and η at 1100°C [(Zandian, Florry et al. 1991)] for type III fused silica, L~75 nm. We note that due to the slow ramp down (0.5°C/min), the sample remains within 90% of the target temperature for an additional time of $\sim\tau/3$; thus it is reasonable to expect features as large as L~100 nm to be significantly smoothed. This estimate is close to the scale of smoothing observed with the nanofibers (<150 nm, Fig. 3).

4.4 Crack closure

The observation of closure of cracks up to 9 μm thick, a dimension larger than that expected to be smoothed by capillary forces alone at this treatment temperature, suggests that another mechanism must be responsible. Crack healing in sapphire crystals has been proposed to occur by blunting of crack tips forming cylindrical voids, then subsequently into spherical pores [(Yen and Coble 1972)]. In that study, it was shown that crack healing was largely driven by surface and volume diffusion, and in related studies it has been shown that thermal healing of these cracks returned the fracture strength of the ceramic to its pre-thermally shocked state [(Gupta 1984)]. Since the cracks in this study were not observed in real-time during anneal, the exact mechanism by which they thermally heal in fused silica was not determined. However, we note that the previously observed transition between the strengthening and weakening regime for indented glass corresponded to a value of $t/\tau \sim 10^5$ [(Hrma, Han et al. 1988)]; in the present study our anneal protocol yields $t/\tau \sim 10^3$, well within the strengthening regime. Thus, the significant decrease in the growth rate following

anneal is associated with an increase in fracture toughness of the initiated sites. We hypothesize that the thermally-driven closure of cracks leaves the site in a more plastically deformed (less brittle) state, permitting the bulk to absorb more of the energy transferred from the laser pulse, thereby reducing the amount of subsequent fracture (and hence resulting size of the grown damage site) than would arise had these cracks not been healed. Figure 4 illustrates how this effect is more pronounced in the smaller, as-initiated sites by the healing of thinner, narrower cracks readily achievable by capillary flow at this anneal temperature; the larger sites instead have a much more complex fracture structure which frustrates relaxation. This effect is short-lived, as 2 more growth shots render the annealed site with a growth rate as if there were no anneal; it is possible that at this stage, the originally damaged volume has been ejected as the site is grown and fresh cracks have been introduced. Further studies tracking the evolution of the crack network within the bulk is necessary to validate this hypothesis.

In conclusion, the major difference between as-initiated and grown damage sites observed in this study is the existence of large cracks in the growing sites which were too wide to heal under the present protocol; after anneal, the large sites still contained cracks which make the site weaker than the smaller sites, rendering large sites prone to larger growth events. In failure analysis, for a material with a given crack distribution, the largest crack in the distribution is the weakest mechanically and thus considered the limiting factor in mechanical failure. At even higher temperatures, as the glass becomes less viscous, it is expected that the material will relax under capillary flow, fusing these wider cracks.

Acknowledgments

The authors would like to acknowledge William Steele, Ted Laurence, David Cross and the OSL team for assistance with sample preparation and growth experiments. This work performed under the auspices of the U.S. Department of Energy by Lawrence Livermore National Laboratory under Contract DE-AC52-07NA27344.

REFERENCES

[1] Atherton, L. J., Rainer, F., De Yoreo, J. J., Thomas, I. M., Zaitseva, N., and F. De Marco (1994). "Thermal and laser conditioning of production- and rapid-growth KDP and KD*P crystals." Proceedings of the SPIE - The International Society for Optical Engineering **2114**: 10.

[2] Brusasco, R. M., B. M. Penetrante, et al. (2002). "Localized CO2 laser treatment for mitigation of 351 nm damage growth on fused silica." Proc. SPIE **4679**: 40-47.

[3] Carr, C., H. Radousky, et al. (2004). "Localized Dynamics during Laser-Induced Damage in Optical Materials." Physical Review Letters **92**(8).

[4] Carr, C. W., D. A. Cross, et al. (2011). "The effect of laser pulse shape and duration on the size at which damage sites initiate and the implications to subsequent repair." Optics Express **19**(14): A859-A864.

[5] Carr, C. W., M. J. Matthews, et al. (2007). The effect of laser pulse duration on laser-induced damage in KDP and SiO2 - art. no. 64030K. Laser-Induced Damage in Optical Materials: 2006. G. J. Exarhos, A. H. Guenther and K. L. Lewis. **6403:** K4030-K4030.

[6] Carr, C. W., J. B. Trenholme, et al. (2007). "Effect of temporal pulse shape on optical damage." Applied Physics Letters **90**(4).

[7] Corning, I. (2003). HPFS(R) Fused Silica Standard Grade.

[8] Dahmani, F., J. C. Lambropoulos, et al. (1999). "Fracture of fused silica with 351 nm laser-generated surface cracks." Journal of Materials Research **14**(2): 597-605.

[9] Devine, R. A. B. (1990). "ON THE PHYSICAL MODELS OF ANNEALING OF RADIATION-INDUCED DEFECTS IN AMORPHOUS SIO2." Nuclear Instruments & Methods in Physics Research Section B-Beam Interactions with Materials and Atoms **46**(1-4): 261-264.

[10] Genin, F. Y., A. Salleo, et al. (2001). "Role of light intensification by cracks in optical breakdown on surfaces." J. Opt. Soc. Am. A **18**(10): 2607-2616.

[11] Gupta, T. K. (1984). Crack healing in Al2O3, MgO, and related materials. Advances in Ceramics. W. D. Kingery, American Ceramic Society**:** 750-766.

[12] Hrma, P., W. T. Han, et al. (1988). "THERMAL HEALING OF CRACKS IN GLASS." Journal of Non-Crystalline Solids **102**(1-3): 88-94.

[13] Hu, G., Y. Zhao, et al. (2010). "Studies of laser damage morphology reveal subsurface feature in fused silica." Surface and Interface Analysis **42**(9): 1465-1468.

[14] Huang, W.-Q., W. Han, et al. (2009). "Laser-Induced Damage Growth on Larger-Aperture Fused Silica Optical Components at 351 nm." Chinese Physics Letters **26**(1).

[15] Juodkazis, S., M. Watanabe, et al. (2000). "Optically induced defects in vitreous silica." Applied Surface Science **154**: 696-700.

[16] Kucheyev, S. O. and S. G. Demos (2003). "Optical defects produced in fused silica during laser-induced breakdown." Applied Physics Letters **82**(19): 3230-3232.

[17] Laurence, T. A., J. D. Bude, et al. (2012). "Extracting the distribution of laser damage precursors on fused silica surfaces for 351 nm, 3 ns laser pulses at high fluences (20-150 J/cm 2)." Optics Express **20**(10): 11561-11573.

[18] Laurence, T. A., J. D. Bude, et al. (2009). "Metallic-like photoluminescence and absorption in fused silica surface flaws." Applied Physics Letters **94**(15).

[19] Matthews, M. J., J. S. Stolken, et al. (2009). "Residual stress and damage-induced critical fracture on CO 2 laser treated fused silica." Proceedings of the SPIE - The International Society for Optical Engineering **7504**: 750410 (750412 pp.)-750410 (750412 pp.).

[20] Menapace, J. A., B. Penetrante, et al. (2002). "Combined advanced finishing and UV-laser conditioning for producing UV-damage resistant fused silica optics." Proc. SPIE **4679**: 56-68.

[21] Milam, D., W. H. Lowdermilk, et al. (1982). "INFLUENCE OF DEPOSITION PARAMETERS ON LASER-DAMAGE THRESHOLD OF SILICA TANTALA AR COATINGS." Applied Optics **21**(20): 3689-3694.

[22] Mullins, W. W. (1959). "FLATTENING OF A NEARLY PLANE SOLID SURFACE DUE TO CAPILLARITY." Journal of Applied Physics **30**(1): 77-83.

[23] Negres, R. A., G. M. Abdulla, et al. (2012). "Probability of growth of small damage sites on the exit surface of fused silica optics." Optics Express **20**(12): 13030-13039.

[24] Negres, R. A., M. A. Norton, et al. (2010). "Growth behavior of laser-induced damage on fused silica optics under UV, ns laser irradiation." Optics Express **18**(19): 19966-19976.

[25] Negres, R. A., M. A. Norton, et al. (2009). "The effect of pulse duration on the growth rate of laser-induced damage sites at 351 nm on fused silica surfaces." Proceedings of the SPIE - The International Society for Optical Engineering **7504**: 750412 (750410 pp.)-750412 (750410 pp.).

[26] Norton, M. A., L. W. Hrubesh, et al. (2001). Growth of laser initiated damage in fused silica at 351 nm. Laser-Induced Damage in Optical Materials: 2000, Proceedings. G. J. Exarhos, A. H. Guenther, M. R. Kozlowski, K. L. Lewis and M. J. Soileau. **4347:** 468-468.

[27] Nostrand, M. C., T. L. Weiland, et al. (2003). A large aperture, high energy laser system for optics and optical component testing. Laser-Induced Damage in Optical Materials: 2003. G. J. Exarhos, A. H. Guenther, N. Kaiseret al. **5273:** 325-333.

[28] Parikh, N. M. (1958). "EFFECT OF ATMOSPHERE ON SURFACE TENSION OF GLASS." Journal of the American Ceramic Society **41**(1): 18-22.

[29] Primak, W. and H. Szymanski (1956). "RADIATION DAMAGE IN VITREOUS SILICA - ANNEALING OF THE DENSITY CHANGES." Physical Review **101**(4): 1268-1271.

[30] Raman, R. N., M. J. Matthews, et al. (2010). "Monitoring annealing via CO2 laser heating of defect populations on fused silica surfaces using photoluminescence microscopy." Optics Express **18**(14): 15207-15215.

[31] Raze, G., J. M. Morchain, et al. (2003). "Parametric study of the growth of damage sites on the rear surface of fused silica windows." Proceedings of the SPIE - The International Society for Optical Engineering **4932**: 127-135.

[32] Scherer, G. W. (1992). Relaxation in Glass and Composites, Krieger.

[33] Shen, N., Miller, P. E., Bude, J. D., Laurence, T. A., Suratwala, T. I., Steele, W. A., Feit, M. D., and L. L. Wong (2012). "Thermal annealing of laser damage precursors on fused silica surfaces." Optical Engineering **51**: 121817.

[34] Skuja, L. (1998). "Optically actice oxygen-deficiency-related centers in amorphous silicon dioxide." Journal of Non-Crystalline Solids **239**: 16-48

[35] Suratwala, T. I., P. E. Miller, et al. (2011). "HF-Based Etching Processes for Improving Laser Damage Resistance of Fused Silica Optical Surfaces." Journal of the American Ceramic Society **94**(2): 416-428.

[36] Swain, J. E., S. E. Stokowski, et al. (1982). "THE EFFECT OF BAKING AND PULSED LASER IRRADIATION ON THE BULK LASER DAMAGE THRESHOLD OF POTASSIUM DIHYDROGEN PHOSPHATE CRYSTALS." Applied Physics Letters **41**(1): 12-14.

[37] Temple, P. A., W. H. Lowdermilk, et al. (1982). "Carbon dioxide laser polishing of fused silica surfaces for increased laser-damage resistance at 1064 nm." Applied Optics **21**(18): 3249-3255.

[38] Tian, G. L., J. B. Huang, et al. (2005). "Microstructure and laser-induced damage threshold of ZrO2 coatings dependence on annealing temperature." Applied Surface Science **239**(2): 201-208.

[39] Wong, J., J. L. Ferriera, et al. (2006). "Morphology and microstructure in fused silica induced by high fluence ultraviolet 3 omega (355 nm) laser pulses." Journal of Non-Crystalline Solids **352**(3): 255-272.

[40] Yang, S. T., M. J. Matthews, et al. (2010). "Comparing the use of mid-infrared versus far-infrared lasers for mitigating damage growth on fused silica." Applied Optics **49**(14): 2606-2616.

[41] Yen, C. F. and R. L. Coble (1972). "SPHEROIDIZATION OF TUBULAR VOIDS IN AL2O3 CRYSTALS AT HIGH-TEMPERATURES." Journal of the American Ceramic Society **55**(10): 507-&.

[42] Zagoruiko, Y. A. (1999). "Modification of optical properties of ZnSe crystals by means of photothermal treatment." Proceedings of the SPIE - The International Society for Optical Engineering **3578**: 480-483.

[43] Zandian, V., J. S. Florry, et al. (1991). "VISCOSITY OF FUSED-SILICA WITH DIFFERENT HYDROXYL CONTENTS." British Ceramic Transactions and Journal **90**(2): 59-60.